ACADEMIC PRESS

Available online at www.sciencedirect.com

SCIENCE DIRECT®

Journal of Sound and Vibration 263 (2003) 493–514

JOURNAL OF SOUND AND VIBRATION

www.elsevier.com/locate/jsvi

Experiments on the unsteady flow field and noise generation in a centrifugal pump impeller

Jong-Soo Choi*,[1], Dennis K. McLaughlin, Donald E. Thompson

The Pennsylvania State University, University Park, PA 16802, USA

Received 28 November 2000; accepted 27 June 2002

Abstract

This paper reports on an experimental investigation of large-scale flowfield instabilities in a pump rotor and the process of noise generation by these instabilities. Measurements of the fluctuating components of velocity and surface pressure were made with hot-wire probes and surface mounted pressure transducers on a seven bladed back swept centrifugal water pump impeller operating with air as the working fluid. The impeller was operated without a volute or scroll diffuser, thereby eliminating any sound generation from pressure fluctuations on the volute cutoff. Thus the study focused on flow field and noise components other than the blade passage frequency (and its harmonics). The primary goal of the study was to provide fundamental information on the unsteady flow processes, particularly those associated with the noise generation in the device. It was further anticipated that detailed flow measurements would be useful for the validation of future computational simulations.

The measured data at the discharge show a jet-wake type of flow pattern which results in a strong vorticity field. The flow with high velocity found on the pressure side of the impeller tends to move to the low-pressure region present at the suction side of the passage as a form of roll-up around the blade trailing edge. This motion causes an unsteady flow separation at the suction side of the blade and consequently disturbs the flow in the adjacent passage. By interacting with the impeller blades near the trailing edges, this instability flow causes a periodic pressure fluctuation on the blade surface and generates noise by a trailing edge generation mechanism. The spectrum of surface pressure measured at the trailing edge of each blade reveals a cluster of peaks which were identified with azimuthal mode numbers. The correlation between the acoustic farfield pressure and the surface pressure on the impeller blade has proven that the azimuthal modes synchronized with the number of impeller blades generate noise much more efficiently than the other modes. The paper also clarifies the correlation between unsteady flowfield measurements, in both impeller and laboratory co-ordinates, with the radiated noise properties. Thus some light is shed on the noise generation mechanisms of this particular device.

*Corresponding author. Tel.: +82-42-821-6683; fax: +82-42-825-9225.
E-mail address: jchoi@cnu.ac.kr (J.-S. Choi).
[1] Current address: Department of Aerospace Engineering, Chungnam National University, Daejeon, 305-764, Korea

0022-460X/03/$ - see front matter © 2002 Elsevier Science Ltd. All rights reserved.
PII: S0022-460X(02)01061-1

1. Introduction

Centrifugal turbomachines are widely used for their ability to generate relatively high pressure ratios in a short axial distance (compared to axial compressors). They are often found in gas turbine engines, heating, ventilation, and air conditioning systems, and pumps. The motivation for the present study was to develop a better understanding of the hydrodynamic noise generation in centrifugal turbomachinery to guide future quieter designs. Most past flowfield studies were motivated mainly by an interest in producing improved hydrodynamic performance.

In centrifugal turbomachinery, the noise generated is often dominated by tones at the blade passage frequency and higher harmonics. This is a consequence of the strong interaction between the periodic flow discharging radially from the impeller and the stator blades or cutoff leading to the exit duct. A spatially distorted inlet flow field interacting with the rotor may also generate similar tones. In addition to these, broadband noise is generated by trailing edge/flow interaction, turbulent boundary layers and fluctuating separated flow on the impeller blades and housing. Past research has focussed mainly on the generation and reduction of the blade passage frequency tones. Thus, the noise generation mechanism of these tones is relatively well known. Several techniques have been successful in controlling this type of noise. Little work has been done, however, on identifying or reducing the broadband noise sources.

In centrifugal turbomachinery, both types of noise generation mechanisms can occur simultaneously. Tourret et al. [1] have tested a centrifugal pump with a casing and found that the most severe pressure fluctuations occur at the volute cutoff. The efforts aimed at reducing the levels of this interaction noise by changing the impeller and cut-off geometry are summarized in the literature survey by Neise [2]. Embleton [3] has implemented several design changes in the impeller and cutoff, such as sloping the cutoff and impeller blades and including slots in the impeller blades. The approach was, however, based on intuition and a parametric study. A noteworthy advance in reducing the level of blade passage frequency noise from centrifugal fans involves using active source cancellation methods. Neise and Koopmann [4] used a resonator to reduce the blade passage tones by canceling the unsteady aerodynamic noise sources at the cutoff. Later, Koopmann et al. [5] succeeded in reducing the fundamental and harmonics of blade frequency tone by using two phase controlled loud speakers placed at the cutoff.

Compared to the cut-off interaction noise, the sources of broadband noise in turbomachinery are not well understood. It is anticipated that the most severe broadband noise sources are associated with the turbulent flow in the impeller passages and the unsteady discharge flow. In order to understand the broadband noise generation mechanisms therefore, precise knowledge of the flow behavior in the impeller is very important. The *objective* of this study was to develop a fundamental understanding of the unsteady flow field that generates broadband noise in the case of a rotating turbomachine impeller well suited for detailed flow investigations. The ultimate goal was to provide data that would be useful for validation of future modelling efforts such as those undertaken by Dorney et al. [6] and Carolus et al. [7]. Emphasis was placed on the noise sources associated with the impeller independently of the volute cutoff. The *approach* adopted in this research was to determine noise sources by a combination of fluid dynamic and acoustic measurements performed simultaneously.

The overall performance of a centrifugal turbomachine depends not only on the impeller flow but also on the efficiency of the diffuser. The purpose of a diffuser is to recover the kinetic energy

of the discharged flow from the impeller and convert it to static pressure (potential energy). A diffuser may be fitted with vanes depending on the size, speed and pressure ratio of the system [8]. The spatially non-uniform flow discharging from the impeller can induce unsteady flow in the diffuser that can significantly alter the nature of the flow. The nature of the flow unsteadiness is not well known but the flow entering the diffuser has been postulated to interact with the boundary layer on the diffuser walls, and often induce flow separation. The centrifugal impeller discharge flow in both vaned and vaneless diffusers has been investigated in some detail by Inoue and Cumpsty [9].

As discussed above, the presence of a vaneless or vaned diffuser influences the flow field inside of the impeller passages, which makes it difficult to understand the nature of the flow. Since a major portion of this research was to characterize the flow field discharging from a centrifugal impeller, the impeller was tested without a diffuser or casing. In addition to developing some fundamental understanding, the study may have indirect applications to the class of centrifugal turbomachines that collect the discharged fluid without a cutoff on the volute and without diffuser stator vanes. The effect of discharge configurations on the flow field was examined in a parallel study and reported by Bent [10]. The study of Bent [10] and the earlier study reported by Mongeau et al. [11] both used the same facility as the present experiments. The Mongeau et al. [11] experiments focused on the acoustic measurements whereas the current study focuses more on the flow field (and the noise generators). Follow-on work using this facility by Tetu [12] and later by Carolus et al. [17] report on studies focusing on more specific aspects of the phenomena investigated in this work.

In turbomachinery, there are several non-dimensional parameters governing the flowfield aeroacoustics. Among these, the most important to this study are the flow coefficient φ, and the static pressure rise coefficient mentioned earlier, ψ as well as the Mach number ($M = V_{tip}/a$) and Reynolds number ($Re_D = V_{tip}D/v$). At 3000 r.p.m. the impeller tip speed reaches $M = 0.15$ and the Re_D is 1.0×10^6 when operating in air. Flow compressibility effects are therefore considered negligible with air as the fluid medium.

2. Experimental facility and procedure

2.1. Main experimental facility

As mentioned earlier, in this study aerodynamic and acoustic measurements were performed on a centrifugal water pump using air as the fluid medium. There are advantages to performing experiments using air instead of water, such as easier operation, more availability of appropriate instrumentation, and simpler test set-up (as shown by Gilman [13]). Further details on the influence of different fluid media on the aerodynamic and the acoustic characteristics are summarized in [14].

A commercial water pump impeller (Worthington Model D-1011) was chosen for the experiments (shown schematically in Fig. 1). The impeller has seven backward swept blades with a discharge angle of about 21° to the tangent. The impeller has a curved front shroud while the hub is relatively flat and perpendicular to the inlet flow direction. The inlet and discharge diameters of the impeller are 133.4 and 320.0 mm, respectively. The experimental facility (shown in Fig. 2 and

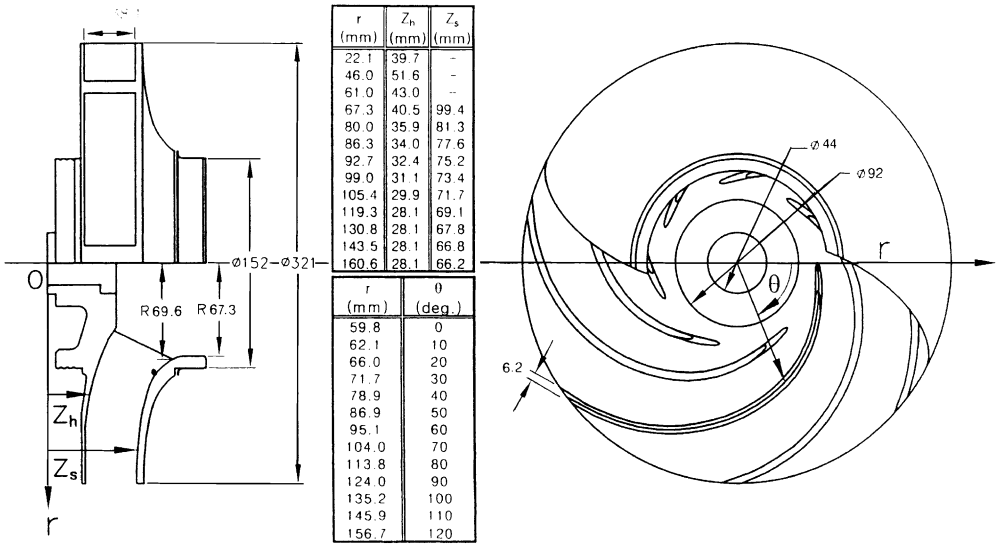

r (mm)	Z_h (mm)	Z_s (mm)
22.1	39.7	-
46.0	51.6	-
61.0	43.0	-
67.3	40.5	99.4
80.0	35.9	81.3
86.3	34.0	77.6
92.7	32.4	75.2
99.0	31.1	73.4
105.4	29.9	71.7
119.3	28.1	69.1
130.8	28.1	67.8
143.5	28.1	66.8
160.6	28.1	66.2

r (mm)	θ (deg.)
59.8	0
62.1	10
66.0	20
71.7	30
78.9	40
86.9	50
95.1	60
104.0	70
113.8	80
124.0	90
135.2	100
145.9	110
156.7	120

Fig. 1. Tested centrifugal pump impeller.

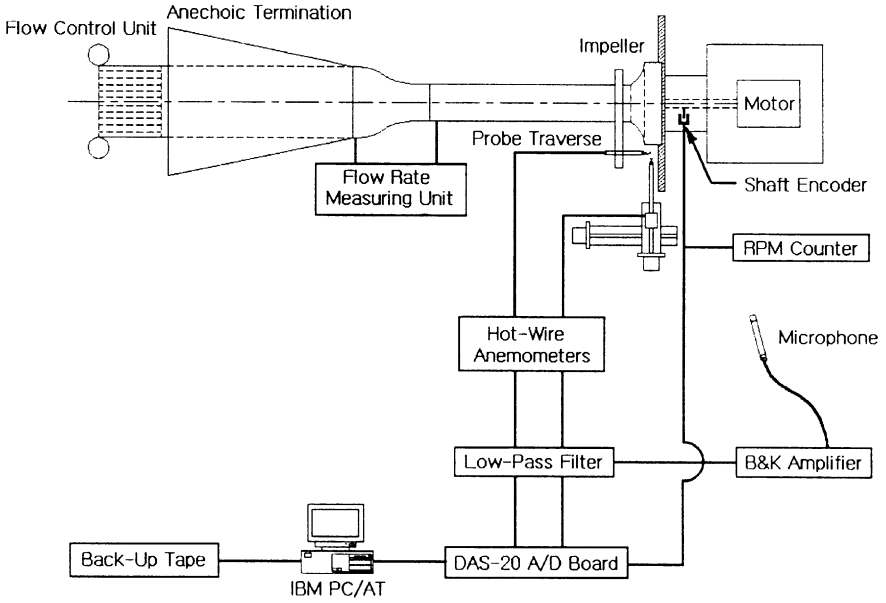

Fig. 2. Test set-up and data acquisition system.

discussed in earlier work by Mongeau et al. [11]) was designed for the quiet operation of a centrifugal turbomachine without an outer casing. A quiet drive system is used to power the impeller at any rotational speed up to 3600 r.p.m. The rotational speed of the impeller is measured with an optical shaft encoder placed between the motor and the bearings. The shaft encoder emits

a 5 V pulse every revolution as well as more finely spaced smaller pulses. In the present experiments, the once per revolution pulse is sampled simultaneously with the other signals from the sensors.

The inlet flow is controlled by an upstream flow management unit, including a bellmouth inlet, turbulence management screens, honeycomb and a duct. Part of the upstream ducting is also an anechoic termination that is used to minimize acoustic reflections from the inlet of the duct. A streamlined contraction is positioned between the two different size plastic ducts connecting the anechoic termination to the impeller. Besides matching the flow areas the contraction also reduces the turbulence level of the flow coming from the upstream flow management unit. A pitot-tube as well as a hot-wire probe survey upstream of the pump inlet showed that the inlet flow was free of pulsations and had a velocity profile that was uniform in the middle except for a relatively thick boundary layer annulus [14]. The volumetric flow rate Q was determined by applying Bernoulli's equation to the static pressure difference and the cross-sectional area ratio measured at the neckdown. Noise propagating up the inlet duct was measured with two flush mounted B&K condenser microphones (Model 4181). The acoustic impedance at the inlet duct was also measured with these microphones and reported in great detail by Mongeau et al. [15]. All experiments were conducted in the anechoic chamber of the Center for Acoustics and Vibration at the Pennsylvania State University.

The impeller performance characteristics were determined from the static pressure difference (Δp) between the impeller inlet and the discharge, at various flow rates. The non-dimensional static pressure rise through the impeller ($\psi = \Delta p/\rho V_{tip}^2$), plotted versus flow coefficient ($\varphi = Q/\pi bDV_{tip}$) constitutes the non-dimensional operating curve for the impeller. The curves at two different shaft speeds collapse well which suggests that the non-dimensional parameters have been properly chosen (Fig. 3). From manufacturer's data it was determined that the impeller was originally designed to have a maximum efficiency at $\varphi = 0.062$. Extensive flow measurements were performed over a range of flow rates at $\varphi = 0.06$ (low flow rate), $\varphi = 0.09$ (medium) and $\varphi = 0.12$ (high flow rate).

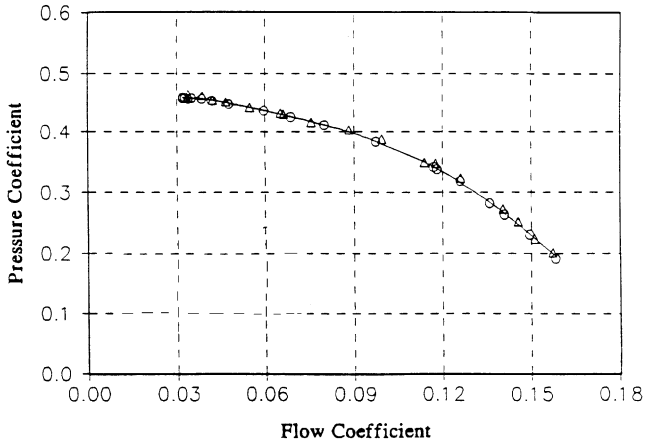

Fig. 3. Non-dimensional performance characteristics of the impeller: ○, $n = 2400$ r.p.m.; △, $n = 3000$ r.p.m.

2.2. Instrumentation

Hot-wire sensors are ideal for the measurement of turbomachinery flows because of their high frequency response, low noise level, and fine spatial resolution. In the experiment described below, the unsteady discharge flow field was measured with both single and crossed hot-wire probes (both of which use five micrometer Walleston wire). The crossed-wire probe calibration procedure and data processing techniques used in these experiments follow those of Westphal and Mehta [16].

All hot-wire probes were calibrated up to 30 m/s in a small wind tunnel using a pitot-static probe as the standard. This velocity range was found to be suitable for the discharge flow tested in this research. Once the probe was calibrated, a check was made on its accuracy by varying the probe angle in the calibration jet and comparing the estimated velocity with the true velocity. The measuring accuracy of the velocity magnitude and yaw angle are $\pm 2\%$ and $\pm 2^{\circ}$, respectively, for yaw angles up to $\pm 35^{\circ}$. Probes were recalibrated several times to check the repeatability of the calibration, which was normally very good.

Several problems may be encountered in the use of multi-sensor probes of the type used in this study. For example, when using a two velocity component sensitive hot-wire probe in a three-dimensional flow field, such as the discharge of a centrifugal turbomachine, the velocity estimation may be contaminated by the out of plane third velocity component. Also, the spatial resolution of the crossed-wire probe, which is about 2 mm, may not be adequate. This is a problem if the flow has a strong spatial non-uniformity. To determine the degree of contamination by the axial velocity component, the crossed-wire data taken near the impeller discharge were compared with single-wire data measured at the same location. Considering the aforementioned limitations in using cross-wire probes, the observed relative errors of less than $\pm 5\%$ were considered quite reasonable.

In addition to the discharge flow measurement, the velocity in the rotating frame was measured with a hot-wire mounted on the impeller. The probe body consisted of an 8 mm long ceramic tube with two small holes in which two 12 mm long parallel, gold plated needles are supported. The same 5 μm wire used for the stationary hot-wire sensors was soldered at the tip of the needles. The small size and mass of the probe made it possible to operate the impeller with the probe attached at speeds up to 2400 r.p.m. (without unbalancing the impeller).

The lead wires from the hot-wire probe were connected to a slip-ring unit mounted on the impeller shaft. The slip-ring unit used in this experiment, Model IECFCS-2-10 by IEC Corporation, has 10 channels and each channel has four silver graphite contacts for signal transmission. The hot-wire anemometer bridge was balanced and calibrated with and without the slip-ring unit and shows identical calibration characteristics in both cases. It has been shown by Hah and Lakshminarayana [17] under similar conditions that the effects of centrifugal forces of the rotating hot-wire on the calibration is negligible. In their experiment, the rotation of the probe was varied from 800 to 1200 r.p.m. which corresponds to a centrifugal acceleration of 500 to 700$\boldsymbol{g}$. In the present experiments, data taken over a range of rotational speed (up to 2400 r.p.m.) collapse very well when properly scaled. Therefore, in the present experiments, no adverse effects of the hot-wire rotation on its output is expected.

To measure the unsteady static pressure on impeller blades, pressure transducers manufactured by the PCB Corporation (model 103A11) were selected. The sensor has a cylindrical shape,

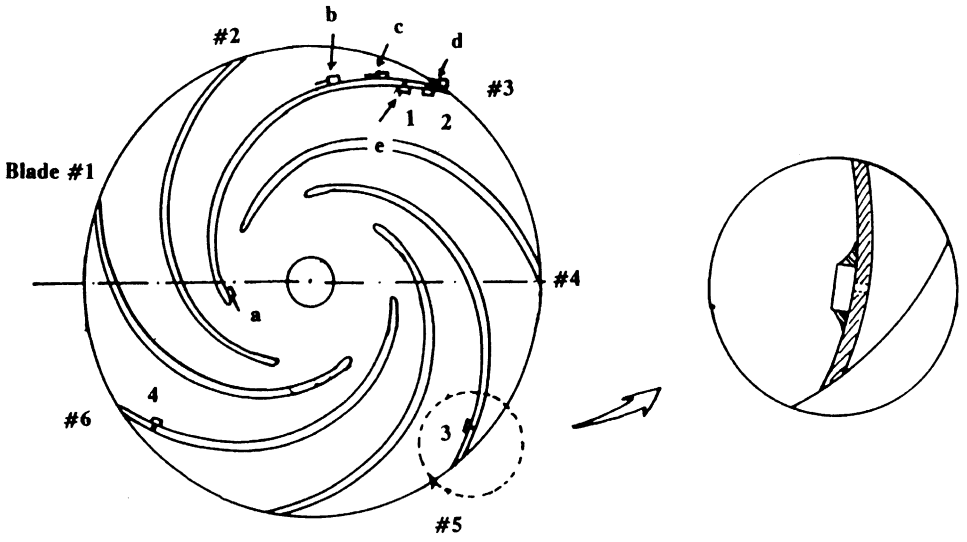

Fig. 4. Sensor locations.

9.4 mm in diameter and 5.6 mm in height, and 2.3 g in mass. Only the unsteady component of pressure is measured, because of the characteristics of the piezoceramic materials used in the sensor. The sensor has a built-in amplifier and vibration compensating accelerometer which produces a high signal-to-noise ratio. The small size, high sensitivity and high frequency response of the sensor have proven to be adequate for this application.

As illustrated in Fig. 4, the impeller blade surface pressure is measured by a sensor attached to the opposite side of an impeller blade through a 2.5 mm diameter pinhole. The resonance frequency of the cavity inside the pinhole was estimated to be 20 kHz. The pinhole was covered with aluminum tape to determine the noise level of the sensor signal due only to mechanical and electrical sources during impeller operation. In a typical experiment, the signal-to-noise ratio is more than 15 dB for the frequency range of interest (between 100 and 800 Hz).

A digital data acquisition and analysis system based on an IBM PC compatible computer and a Metrabyte DAS-20 12 bit A/D converter was used to acquire and analyze data. The analog signals from the sensors were monitored on a Tektronix Storage Oscilloscope Model 2230 and Hewlett Packard Frequency Analyzer 35660A. To avoid aliasing problems in digital signal processing, low pass analog filters (Ithaco Model 4302) were used in all measurements. Further details on the experimental facility and noise measurement techniques are reported in Choi [14] and Mongeau et al. [11].

2.3. *Phase averaging and co-ordinate transformation*

The hot-wire data measured at the impeller discharge have strong periodicity at the impeller blade rate. This was determined from the measured signal by using a synchronous averaging technique in which all hot-wire data are sampled in conjunction with a signal from the shaft encoder. This technique decomposes a measured instantaneous flow velocity (v) into a

circumferential mean ($\overline{V}$), an averaged spatial variation ($\tilde{V}$), and perturbation on top of these mean values (v'),

$$v(\theta, t) = \bar{V} + \tilde{V}(\theta) + v'(\theta, t), \tag{1}$$

where bold symbols imply that each term is a vector quantity.

The $\tilde{V}$ is periodic at the synchronizing frequency (shaft rate) and has zero mean value. The perturbation term (v') therefore represents any flow unsteadiness not synchronized with the shaft rate. In contrast to the time dependent (v'), the remaining two ensemble averaged values can be represented with a single time independent parameter V,

$$V(\theta) = \overline{V} + \tilde{V}(\theta). \tag{2}$$

This mean value V is a function of azimuthal location and will be used hereafter to represent the phase averaged mean velocity at the discharge.

For digitally sampled data the phase-averaged velocity can be calculated as

$$V(\theta) = V(i\Delta t) = \frac{1}{N}\sum_{k=1}^{N} v(i\Delta t, k), \quad i = 0, 1, 2, \ldots, N, \tag{3}$$

where N is the number of averages and Δt is the sampling interval. Similarly, the root mean square value of the fluctuating velocity can be obtained as

$$v'_{r.m.s.}(\theta) = v'_{r.m.s.}(i\Delta t) = \sqrt{\frac{1}{(N-1)}\sum_{k=1}^{N}[v(i\Delta t, k) - V(i\Delta t)]^2}, \quad i = 0, 1, 2, \ldots, N. \tag{4}$$

In this procedure the velocity data at $i = 0$ corresponds to the data sampled when the shaft encoder gives a reference pulse signal. The averaging technique significantly reduces the random fluctuations superposed on the periodic signal. The mean velocity data presented in this paper are averaged over 100 impeller revolutions, since taking more than 100 averages produced little effect on the averaged data.

The velocity distribution information is more easily understood by converting the measured data from the laboratory co-ordinate frame to a frame of reference on the impeller. In this transformation, the radial component of the velocity is identical in both the stationary and rotating co-ordinate frames. The tangential component in impeller co-ordinates is found from the relationship

$$U_t = (R + \Delta r)\Omega - V_t \equiv r\Omega - V_t, \tag{5}$$

where Ω is the angular rotational speed of the impeller, R is the impeller radius, Δr is the radial distance from the impeller trailing edge; so $r = R + \Delta r$.

2.4. Processing of unsteady hot-wire and microphone data

The power spectral densities processed from microphone, hot-wires, and pressure transducer signals are normalized with the following parameters: the square of the impeller tip speed is used for the power spectral density of velocity G_{uu}, and dynamic pressure based on V_{tip} is used for the power spectral density of the pressure fluctuations G_{pp}. The resulting non-dimensional power

spectral densities are

$$L_{uu}(St) = 10\log[G_{uu}(f)/V_{tip}^2(D/V_{tip})], \quad L_{pp}(St) = 10\log[G_{pp}(f)/\rho_0^2 V_{tip}^4(D/V_{tip})], \qquad (6,7)$$

where the frequency is non-dimensionalized with the blade passage frequency to form the Strouhal number. For the experiments reported here, the blade passage frequency was in the range from 280 to 420 Hz.

A scaling factor D/V_{tip} is introduced in Eqs. (4) and (5) to accompany switching the independent variable from a frequency (f) to a Strouhal number (St). For the spectra presented in this paper, the number of data (N) was 1024 and the sampling frequency was 2 kHz for each channel, so the frequency bin width was 1.95 Hz. One hundred averages were performed with a 50% overlap and a Hanning window was used to taper each 1024 data record.

3. Experimental results and discussion

3.1. Character of mean flow in an impeller passage

Fig. 5 shows the synchronous averaged discharge velocity magnitude in the stationary (laboratory) co-ordinate frame at various radial positions. These data transformed into the impeller co-ordinate frame are shown in Fig. 6. The probe was placed at mid-passage, i.e., $z/b = 0.5$, and the impeller was operated at the presumed maximum efficiency flow rate $\varphi = 0.06$.

The impeller tip speed is used to non-dimensionalize these quantities. The horizontal scale, marked as a fraction of a revolution, begins at the trailing edge of impeller blade no. 1. The locations of the second blade trailing edge, is marked with a vertical dotted line. The pressure and suction sides of each blade are marked with P and S on opposite side of the dotted lines,

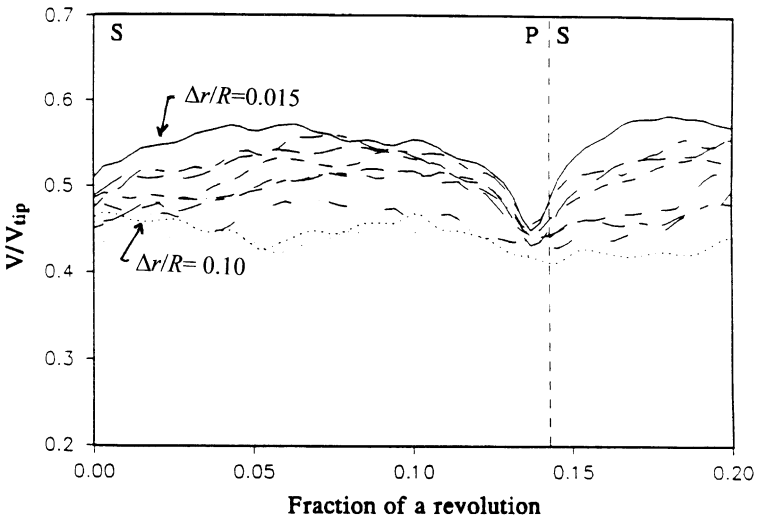

Fig. 5. Measured discharge velocity amplitudes at various radial locations in stationary co-ordinates ($\varphi = 0.06$, $z/b = 0.5$): $\Delta r/R = 0.015$, 0.02, 0.025, 0.03, 0.04, 0.05, …, 0.10.

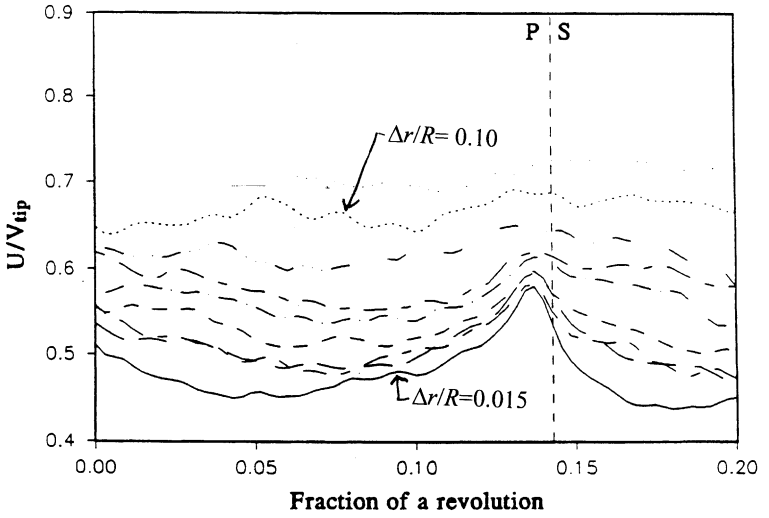

Fig. 6. Measured discharge velocity amplitudes at various radial locations in rotating co-ordinates ($\varphi = 0.06$, $z/b = 0.5$): $\Delta r/R = 0.015$, 0.02, 0.025, 0.03, 0.04, 0.05, …, 0.10.

respectively. The pressure side corresponds to the convex side of a blade, because the blades are swept backward.

The discharge velocity pattern (in rotating co-ordinates), plotted in Fig. 6, clearly shows a high velocity (jet) region near the pressure side of a blade compared to the low velocity (wake) region in the suction side. This jet and wake type of flow pattern has been observed by many other investigators in centrifugal turbomachinery experiments (Maksoud and Johnson [18], Dean and Senoo [19], Fowler [20], Eckardt [21], Johnson and Moore [22] and Carolus et al. [7]).

The most striking feature of the synchronous averaged velocity profiles is, however, the apparent width of the wake (in the jet/wake velocity profile). Rather than a near wake made up of two shed boundary layers from the two sides of the impeller blade, the suction side wake appears to occupy nearly one half of the channel depth. This is strong evidence that secondary flows convect the low momentum fluid from the suction side of the boundary layer into the mid passage area giving the "appearance" of a greatly increased wake width.

At all three flow rates, the discharge flow field shows a highly sheared region near the trailing edge of each blade where mixing occurs between the jet that is adjacent to the pressure side surface of the blade and the apparently broad wake (of the blade). This flow mixing is so rapid that the jet-wake pattern cannot be identified at radial locations greater than 1.1 times the impeller radius. The measurements taken at the closest location to the impeller, $\Delta r/R = 0.015$, show the jet-wake flow structure clearly for all three flow rate cases. The region near the suction side of the trailing edge, however, does not show a defined blade wake emanating from the trailing edge. Similar observations have been made by Maksoud and Johnson [18] and CFD computations of Carolus et al. [7] are consistent with these measurements.

The jet-wake flow pattern can be more clearly identified with the velocity contours shown in Fig. 7. Three flow rate cases are compared for the measurements taken with the crossed-wire probe over roughly one impeller passage. For each figure the velocity data are measured at seven equally spaced axial locations from hub to shroud are used (after transformation to rotating

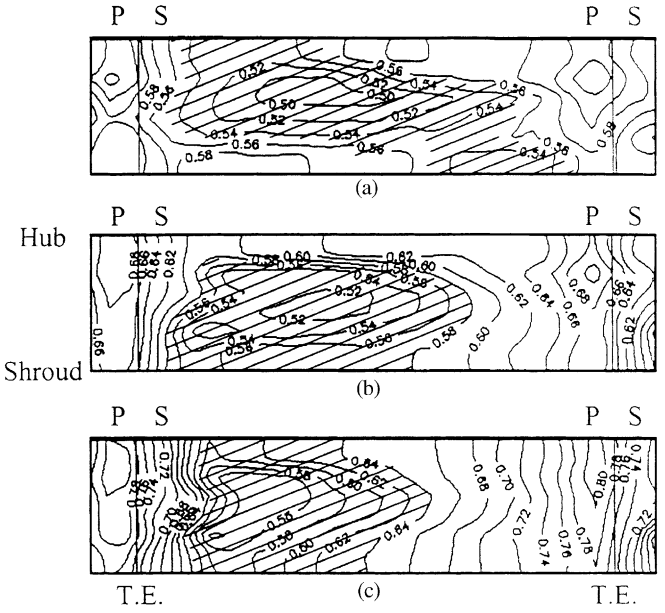

Fig. 7. Relative velocity contours ($\Delta r/R = 0.02$). (a) $\varphi = 0.06$; (b) $\varphi = 0.09$; (c) $\varphi = 0.12$.

co-ordinates). The contour levels below the spatial mean velocity are shaded in the figure to show the low velocity region. At low flow rate $\varphi = 0.06$, the wake region is located in the middle of the passage while the high velocity region is confined near the hub/pressure-side corner. In contrast, when the flow rate is increased to $\varphi = 0.12$, a distinct wake region is developed near the shroud adjacent to the suction surface of the blade, and the jet region dominates half of the pressure side of the passage.

When the jet side flow passes near the trailing edge of a blade, the angle becomes smaller due to the lower pressure on the suction side of the blade. This is shown in Fig. 8 with the phase averaged discharge angle of the flow. The flow angles, relative to the tangent, are shown at three radial locations for a flow rate of $\varphi = 0.06$. The discharge angle in rotating co-ordinates is much less than the blade angle (which is 21° to the tangent). The flow angle shows substantial variation along the impeller circumference when it is measured close to the impeller. This spatial distribution of flow angle quickly becomes uniform as the flow moves outwards from the impeller. A high discharge angle (between 10° and 15°) is found in the jet region, while the angle near the wake is very small (about 5°). The region immediately behind the trailing edge has the smallest flow angle and the fastest change in flow angle. These accelerations no doubt play a major role in the generation of noise by the flow.

From the measured velocity magnitude and angle, the radial and tangential component of the discharge velocities can be obtained. The radial velocity is found to be much smaller than the tangential velocity. At $\varphi = 0.06$, as an example, the spatially averaged radial velocity is about 7% of the impeller tip speed compared to the 50% (of tip speed) for the tangential velocity in (rotating co-ordinates).

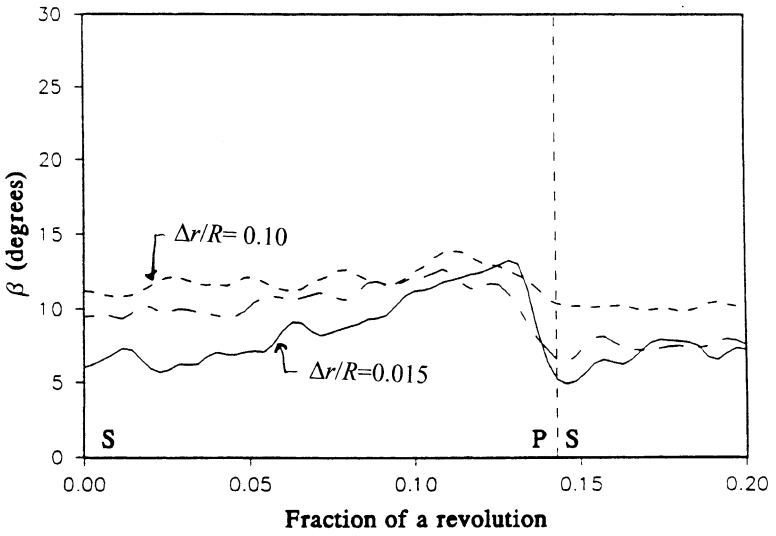

Fig. 8. Measured discharge flow angles at various radial locations in rotating co-ordinates ($\varphi = 0.06$, $z/b = 0.5$): $\Delta r/R = 0.015$, 0.05, 0.10.

3.2. Hot-wire velocity fluctuation measurements

Additional insight on the character of the impeller flow field is obtained from the unsteady or fluctuating portions of the hot-wire signals. For the velocity fluctuation intensity contours shown in Fig. 9 for the $\varphi = 0.09$ medium flow case, fluctuations in tangential and radial velocity components are combined and normalized with the impeller tip velocity. The range of velocity fluctuation intensities at the exit of the blade passage at ($\Delta r/R = 0.02$) is from $v'_{r.m.s.}/V = 0.10$ to 0.25. The high velocity fluctuation region (shaded area) is located where the radial velocity is found to be low. This implies that the high radial velocity region of the flow tends to be more stable than the flow in the low radial velocity region. This may be due to the influence of the adjacent passages, which is more likely to be stronger where the radial velocity is low. From time traces of the instantaneous radial velocity, additional insight into the flow field can be obtained. A negative radial velocity is found intermittently near the suction side and is apparent in all three flow rate cases. This unsteady backflow is believed to disturb the passage flow, and consequently induce the unsteady pressure fluctuation on the blade surface.

It is also found that the overall velocity fluctuation r.m.s. level (normalized) is higher at low impeller flow rates. The low flow momentum through the blade passage, which would promote thick boundary layers on the passage walls, may be responsible for this flow behavior. The boundary layers are spread to the mid channel regions by the secondary flow before reaching the discharge.

3.3. Unsteady flow in an impeller passage

In an attempt to establish how the unstable flow is generated and distributed, a series of hot-wire and unsteady pressure measurements were made in the vane passages. Fig. 10 shows the

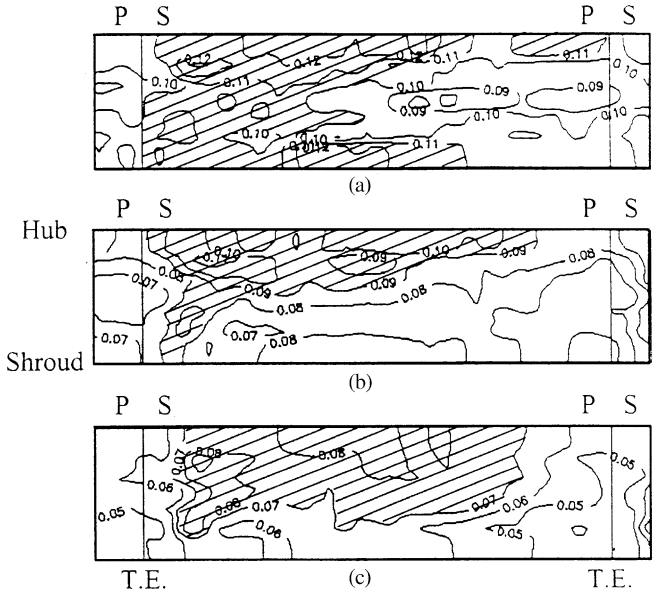

Fig. 9. Turbulence intensity contours ($\Delta r/R = 0.02$). (a) $\varphi = 0.06$; (b) $\varphi = 0.09$; (c) $\varphi = 0.12$.

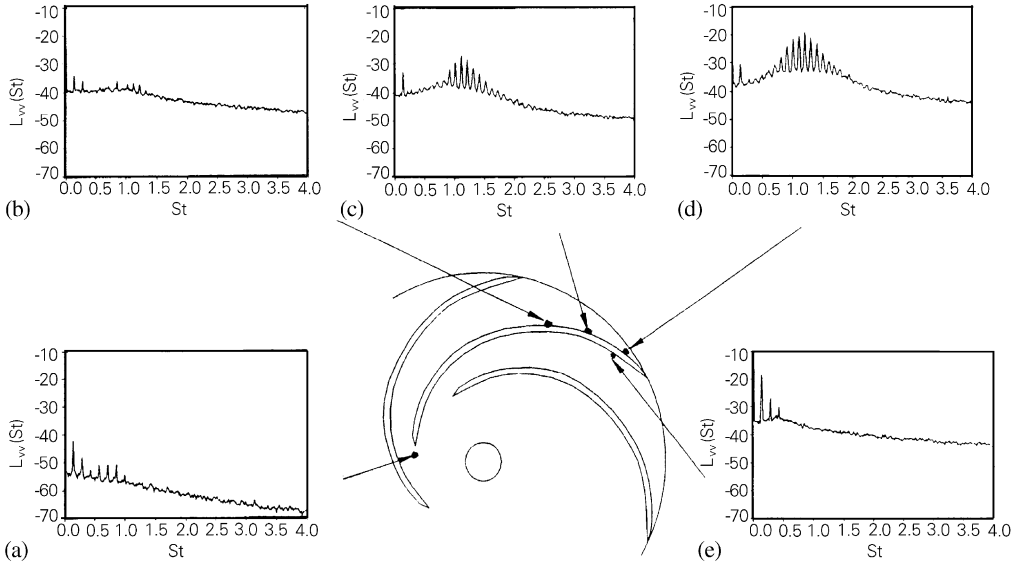

Fig. 10. Velocity spectra measured with a rotating hot-wire at various locations (a) to (e) on an impeller blade ($\varphi = 0.06$, $z/b = 0.5$).

measured spectra with a rotating hot-wire at various locations above a blade surface for the flow rate condition $\varphi = 0.09$. The detailed sensor locations are shown in Fig. 4 and listed in Table 1. For all three cases, a cluster of spectral peaks appears for probe positions near the trailing edge on the pressure side of the blade. The inlet flow spectra measured with a hot-wire sensor at position

Table 1
Relative sensor locations on the impeller blades

Sensor type	Designated label	Sensor locations			
		r/R	S/C*	P or S**	Blade no.
Hot-wire sensors	a	0.35	−0.02	—	3
	b	0.85	0.64	P	3
	c	0.94	0.76	P	3
	d	1.00	1.00	P	3
	e	0.92	0.89	S	3
Pressure transducers	1	0.98	0.89	P	3
	2	0.99	0.95	P	3
	3	0.98	0.89	P	5
	4	0.98	0.89	P	7
	5	0.95	0.89	S	4

*s is measured from the L.E of a blade to the T.E.
**Sensing locations on either pressure or suction.

"a" show low amplitude, or low turbulence level, for all flow rates. The only tones found in the spectra are related to the shaft rate and its harmonics, which are presumably due to the noise from the slip-ring unit and from slight asymmetries in the impeller geometry. The random level of the spectra increases progressively from sensor location "a" to "b" to "c". As can be seen in [14] similar hot-wire spectra were measured at non-dimensional flow rates of $\varphi = 0.06$ and 0.12.

In Fig. 11 is presented the surface pressure spectrum measured with pressure transducer "2" whose pinhole is located just below the rotating hot-wire sensor "d". The gap between the hot-wire and the blade surface was about 5 mm. The similarity in spectral shape of Figs. 11 and 10(d) indicates a strong correlation between the unsteady velocity and the pressure near the surface. In particular, the spectral peaks between Strouhal numbers of 0.5 and 2.0 suggest that a well-organized aerodynamic motion exists that causes a periodic pressure fluctuation on the surface. Each peak in this cluster is separated by a uniform spacing of $\Delta St \approx 0.1$. The cluster is centered about $St \approx 1.2$. In order to distinguish between individual peaks, an integer number is assigned to each of them corresponding to the azimuthal mode number of the spectral component. This number is obtained by dividing the Strouhal number of each peak with the peak spacing. In other words, the peak at $St \approx 0.7$ is named $m = 7$ and the one at $St \approx 0.8$ is $m = 8$, etc.

Mongeau et al. [11] showed that the organized flow motion in one passage is found to be correlated to the unsteady flow in the other passages. The disturbance from a passage propagates over the flow discharged from adjacent passages and creates a coherent flow field around the impeller. Also using a more sophisticated two point cross-spectral analysis technique, Mongeau et al. [11] derived the azimuthal mode numbers of the spectral components derived in this work with the simpler method. More discussion of the organized flow phenomena follows.

Mongeau et al. [11] discuss at some length how the spectral components of the large-scale instability are transformed going from the stationary co-ordinate frame to the rotating frame. This relationship is demonstrated by comparing hot-wire spectra measured with a stationary probe in the impeller discharge (Fig. 12) with the rotating hot-wire measurements shown

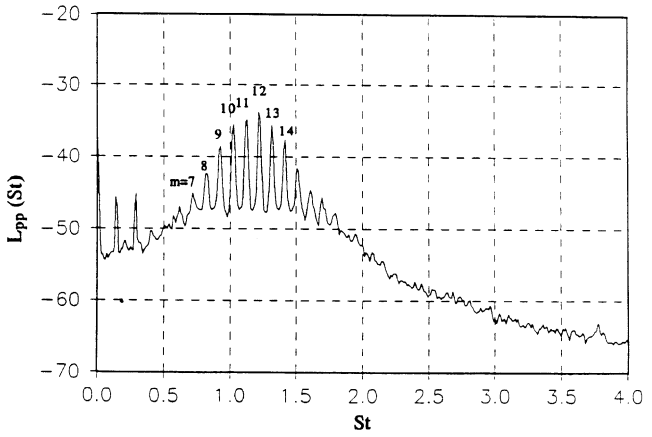

Fig. 11. Power spectral density of pressure near the trailing edge of an impeller blade ($\varphi = 0.09$).

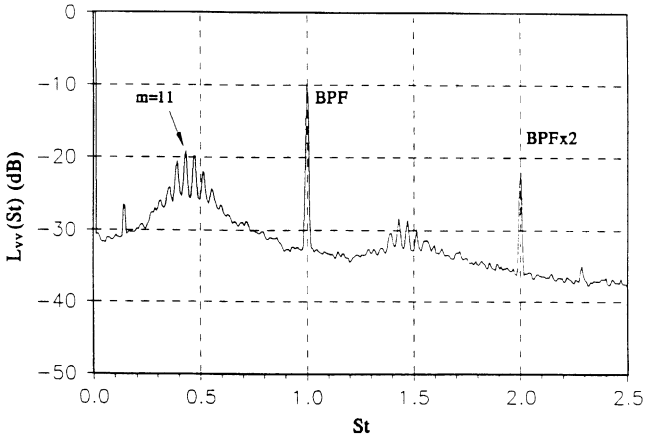

Fig. 12. Spectra of the velocity at impeller discharge ($\varphi = 0.09$, $z/b = 0.5$, $\Delta r/R = 0.02$).

previously (Fig. 10). The frequency component of azimuthal mode no. 11 is shown as one of the highest peaks in the spectrum. As deduced by Mongeau et al. [11] the Strouhal numbers of a mode in both rotating and stationary co-ordinate frames have a relationship as follows:

$$St_S = m/Z - St_R. \tag{8}$$

For example, the Strouhal number of the 11th mode in rotating co-ordinates is $St_R = 1.12$ (shown in Fig. 11), and the corresponding mode appears at $St_S = 0.45$ in the stationary reference frame (Fig. 12). Another feature of a spectrum measured with the stationary probe not present with the rotating probe signals is the presence of the prominent peak at the blade passage frequency (BPF).

3.4. Surface pressure correlation between blades

The influence of large-scale unsteadiness on the adjacent passages can be examined from the cross-spectra of two pressure transducers mounted on different blades. Three pressure sensors,

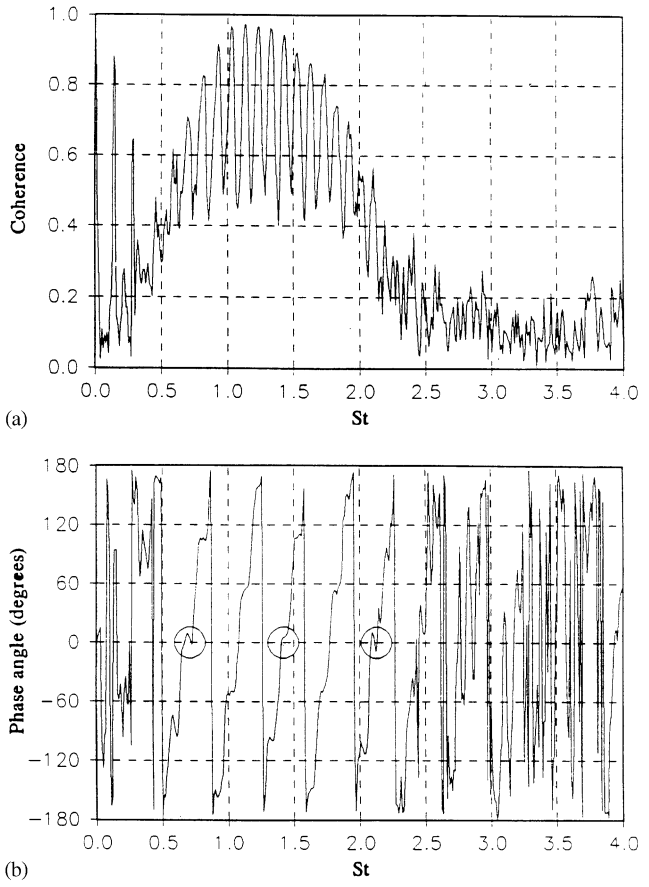

Fig. 13. (a) Coherence and (b) phase angle of cross-spectra between surface pressures at sensor locations 1 and 3 ($\varphi = 0.09$, $z/b = 0.5$).

labeled 1, 3 and 4, were mounted on blades 3, 5 and 7 respectively (Fig. 4). The radial and axial location of these sensors was identical relative to each blade. Shown in Figs. 13(a) and (b) are the coherence and phase angle between sensor 1 and 3, respectively. As shown in Fig. 13(a), the coherence level of those corresponding peaks found in Fig. 11 is more than 0.8. This indicates that the flow disturbances, which generate the peaks in the spectra, are highly correlated between blades even though these blades are separated by two blade passages. A similar result is observed in the coherence between blade 3 and 7 signals, three passages apart.

The unsteady flow that is coherent from blade to blade forms a rotating pattern, and the pattern precesses around the impeller. In a manner similar to the technique used by Mongeau et al. [11] using stationary hot-wire probes, the precessing speed can be estimated from the phase relation between signals from two (rotating) pressure transducers on different blades. Shown in Fig. 13(b) is the phase angle of the cross-spectrum (γ_{13}) between sensor 1 and 3. The approximately linear phase relation between $St = 0.5$ and 2.5 indicates that each mode rotates around the impeller with an almost equal speed. The time delay is estimated from the phase angle and then used with the sensor separation distance measured along the circumference to estimate the wavelength of the

unsteady velocity pattern. The rotational speed (ω) of the pattern at $St = 0.72$ is calculated to be 72% of the shaft rate (Ω) relative to the impeller at the flow rate $\varphi = 0.09$ (and 28% of the shaft rate in the absolute reference frame). It is also found that this normalized rotational speed varies somewhat depending on the flow rate.

It is also important to notice from Fig. 13(b) that the curve crosses the line of zero angle at the frequencies corresponding to the mode numbers which are multiples of the impeller blade number, i.e., $m = 7$, 14, and 21. These points are marked with circles on the figure. There are several additional frequency locations that the curve crosses the zero angle line, which may or may not be related to any integer mode numbers.

3.5. Relationship between the unsteady flow field and the radiated noise

As discussed above, the rotating flow instability at the discharge of the impeller is coupled to the unsteady flow fluctuations in the impeller blade passages. By interacting with the impeller blades, the destabilized passage flow induces unsteady pressure on the blade surface, most prominently near the trailing edges. It is believed that this is a major source of noise. Noise was measured with microphones in both the inlet duct and the acoustic field surrounding the discharge of the impeller. Fig. 14 shows the radiated noise spectrum measured with a microphone in the acoustic far field for the flow rate of $\varphi = 0.09$. In Fig. 14(a) this spectrum is compared with the spectrum of the surface pressure on an impeller blade (pressure sensor 1). The location of the microphone was 2.44 m (8 ft) from the center of the impeller in the same plane as the rotation of the impeller. In the noise spectrum, broad humps appear which are centered at $St \approx 0.7$ and 1.4 and correspond to the first two peaks in the source strength spectral distribution function initially identified by Mongeau et al. [11] in the same facility.

Comparing the noise and the surface pressure spectrum (Fig. 14(a)), it can be seen that the peaks at $m = 7$ and 14 in the surface pressure spectrum generate more acoustic noise than the modes with higher amplitudes ($m = 8, 9, \ldots, 13$). As first described by Mongeau et al. [11], this is due to a near-field pressure cancellation described below. All the modes in the pressure spectrum will generate noise from each blade, but those with mode numbers equal to the number of impeller blades ($m = 7, 14, 21 \ldots$) generate noise that is synchronized. This can be verified from the phase of the cross-spectrum between surface pressures on two separate blades shown in Fig. 13(b). Only the spectral peaks that correspond to multiples of the number of impeller blades are in-phase. All other peaks in the surface pressure cross-spectra are out-of-phase. For example, all seven lobes in the pattern with $m = 7$ induce unsteady pressure on the seven impeller blades simultaneously, or in-phase, while the instability pattern is rotating around the impeller. In contrast to this, the number of lobes in the pattern with $m = 8$ do not match with the number of impeller blades. So, it appears that acoustic waves from different blades interfere with each other and result in relatively less noise propagating to the far field at the frequency. Since the farfield noise in Fig. 14(a) was measured at the plane of the rotating impeller, the noise spectrum at the multiples of blade passage frequency are broader than that of the surface pressure spectrum due to the Doppler effect. It is also expected that the sound pressure level of the spectrum peaks measured at the far field are influenced by the acoustic cancellation due to the non-compact distribution of the sources on seven different impeller blades.

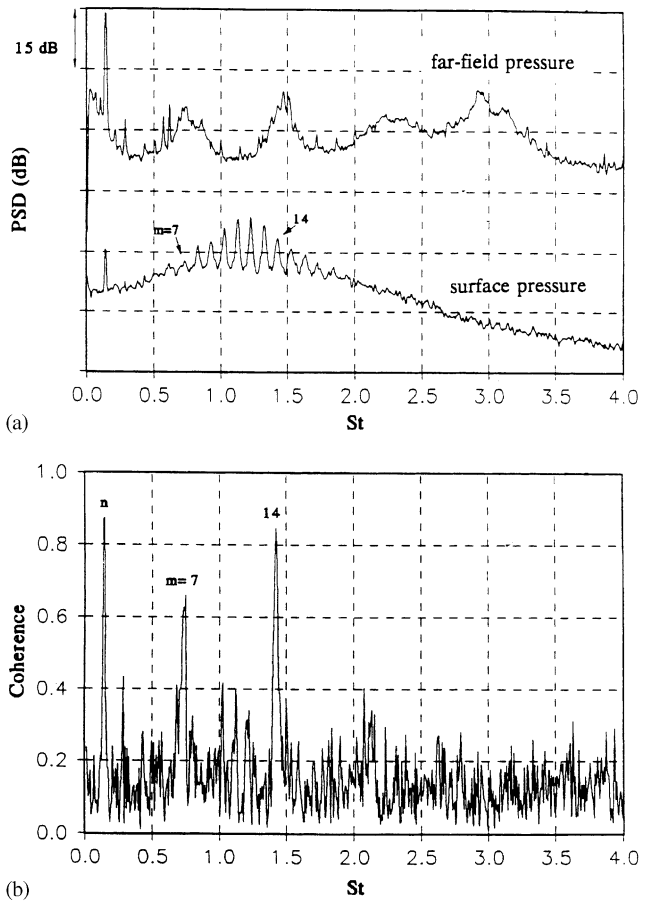

Fig. 14. (a) Farfield noise and surface pressure spectrum and (b) their coherence.

The coherence between the noise and the surface pressure, shown in Fig. 14(b), demonstrates the high correlation level at the frequencies corresponding to $m = 7$ and 14. The peak at $St \approx 0.14$, i.e., shaft rate, in the noise and coherence spectra is generated from the slip-ring unit mounted on the motor shaft. The high coherence level at $m = 7$ and 14 indicates that the peaks in the noise spectrum are generated from the unsteady pressure fluctuation on the impeller blades. In addition, an experiment performed by Mongeau [23] has shown that changes in trailing edge shape affect the generated noise spectra, which further suggests a strong correlation between impeller surface pressure and the radiated noise.

3.6. Discussion

The description and cause of the multi-modal instability in the impeller remains somewhat imprecise. It is quite clear, however, that numerous spectral components have specific azimuthal mode numbers m whose azimuthal "wave lengths" are $360^\circ/m$. As described earlier, the modes with wave numbers $m = 7$, 14 and 21 produce the noise at the trailing edges of the seven impeller

blades synchronously. The noise generation could be described as originating from a non-compact source thus there are variations in retarded times corresponding to observation points not on the axis of the impeller. However, since the range of acoustic wavelengths of the dominant noise is 2 to 3 times the diameter of the impeller, the only manifestation of the non-compact sources and variation in retarded times is relatively minor. Because of some destructive interference, the levels of spectral peaks at off-axis observation points are slightly decreased, an effect that is minimal for on-axis positions.

In depth interpretation of the radiated noise spectra in terms of the blade pressure spectra is beyond the scope of this work. It has been shown however, that the spectral components of the surface pressure fluctuations for which the azimuthal mode number equals multiples of the blade count are expected to be prominent in the noise radiation and that is the case.

Regarding the impeller flow field, the jet-wake flow structure at the impeller discharge permits disturbances on the jet side of the flow to propagate from one passage to the adjacent passage. Flow disturbance migration from one passage to another was also noticed by Fowler [20] who identified an unstable jet-wake pattern at the discharge. The low radial outflow in the wake allowed backflow into this region, and this consequently destabilized the jet-wake flow in the passage. These phenomena were also observed by Dean [24], and were postulated to be a source of noise generation and resonance phenomena acting on the impeller and diffuser channels. However, to the authors' knowledge, no detailed analysis of the relationship between this type of flow and radiated noise has been previously reported.

The unsteady flow phenomenon prominent in this study is similar to rotating stall in a centrifugal impeller or diffuser. However it differs from "conventional stall" in a number of important ways. Firstly, rotating stall typically appears during operation at high back pressures and reduced flow rates. In the present study the instability occurs across the flow rate spectrum and most prominently at medium flow rates around $\varphi = 0.09$, in the middle of the range shown in Fig. 3. Secondly, the number of stalled regions or stall cells is typically on the order of 1 to 4, a number much smaller than the number of impeller blades. In the present study the number of modes of the instability is much greater than the number of impeller blades, and the strongest modes have azimuthal mode numbers in the range from 7 to 18. Finally, in rotating stall, the unsteadiness begins early in the impeller passages, usually at the leading edge of the blades. All of this evidence suggests that the instability present in the current study is not the same as conventional impeller stall and has features that could be found in unstalled centrifugal turbomachinery flow fields. It would not be unreasonable, however, to refer to the instability as a form of mild impeller stall.

4. Conclusions

In this research, an experimental investigation on the unsteady flow field and noise generation mechanism of a centrifugal turbomachine has been performed. The following specific conclusions resulted from the study:

(1) The jet-wake flow pattern found in the impeller blade passages induces a strong vorticity field near the trailing edge of each blade. This vortex is unstable and it influences the

flow discharging from the adjacent passage, and destabilizes the jet-wake flow in the passage.

(2) The unstable passage flow causes a periodic pressure fluctuation on the blade surfaces. This unsteady flow is found to be coherent from blade to blade and forms a rotating instability pattern around the impeller discharge. This instability pattern has a rich harmonic content and a well-defined precessing speed.

(3) The rotating discharge instability in the impeller discharge is very similar in its behavior to the phenomenon known as rotating stall found in centrifugal impellers and diffusers. However, the origin of each of these flows and some of their characters are found to be quite different.

(4) The surface pressure spectrum measured at the trailing edge of each blade revealed a cluster of peaks, which were identified with integer mode numbers. The modes synchronized with the number of impeller blades (mode 7, 14, 21,…) were shown to generate noise more efficiently than the other modes. Consequently, the radiated noise spectra were shown to be dominated by harmonically related broad humps.

Acknowledgements

This research has been supported by the Office of Naval Research through contract N00014-87-K-0837 monitored by Drs. E.P. Rood and L.P. Purtell. The authors would like to acknowledge the assistance of Drs. L. Mongeau and P. Bent in the conduct of this research and the Center for Acoustics and Vibration at Penn State for the use of the anechoic chamber facility.

Appendix A. Nomenclature

a	speed of sound
b	impeller blade width
C	length of the impeller blade along the surface
D	impeller diameter
f	frequency (Hz)
F	acoustic source spectral distribution function
G	acoustic frequency response function
G_{pp}	power spectral density of pressure
G_{uu}	power spectral density of Velocity
He	Helmholtz number, (fD/a)
L_{pp}	non-dimensional power spectral density of pressure
L_{uu}	non-dimensional power spectral density of velocity
m	azimuthal mode number
M	mach number
n	shaft rotational speed (r.p.m)
N	number of data for spectral analysis
Δp	static pressure difference between the impeller inlet and the discharge

p_{ref} reference acoustic pressure (20 μPa)
Q volume flow rate
r radial co-ordinate
R impeller radius
Δr radial distance from the impeller tip
Re_D Reynolds number, $(V_{tip}D/\nu)$
St Strouhal number based on the impeller tip speed, $(\pi D/Z)(f/V_{tip})$
t time (s)
$\boldsymbol{U}$ phase averaged mean velocity vector in rotating co-ordinates
$\boldsymbol{v}$ random velocity component vector in stationary co-ordinates
$\boldsymbol{V}$ phase averaged mean velocity vector in laboratory co-ordinates
V_{tip} impeller tip speed
z axial distance from the shroud
Z number of impeller blades (7)
γ phase angle of a cross-spectrum (deg)
ν kinematic viscosity (m^2/s)
π radians
ρ_o Standard air density ($1.21\,kg/m^3$)
$\Delta\tau$ time delay (s)
φ flow coefficient, $(Q/\pi bDV_{tip})$
ψ pressure rise coefficient, $(\Delta p/\rho V_{tip}^2)$
ω angular rotational speed of the instability pattern (rad/s)
Ω angular rotational speed of the impeller (rad/s)

Subscripts

p pressure
r radial component
$r.m.s.$ root mean squared
R rotating co-ordinates
S stationary co-ordinates
t tangential component

References

[1] J. Tourret, A. Badie-Cassagnet, G. Bernard, J.P. Foucault, J. Kermarec, Experimental studies of noise emission and noise generation from a centrifugal pump, ASME paper No. 95-WA/FE-8, 1985.
[2] W. Neise, Noise reduction in centrifugal fans: a literature survey, Journal of Sound and Vibration 45 (1976) 375–403.
[3] T.F.W. Embleton, Experimental study of noise reduction in centrifugal blowers, Journal of the Acoustical Society of America 35 (1963) 700–705.
[4] W. Neise, G.H. Koopmann, Reduction of centrifugal fan noise by use of resonators, Journal of Sound and Vibration 73 (1980) 297–308.
[5] G.H. Koopmann, D.J. Fox, W. Neise, Active source cancellation of the blade tone fundamental and harmonics in centrifugal fans, Journal of Sound and Vibration 126 (1988) 209–220.

[6] D.J. Dorney, Numerical Simulations of Unsteady Flows in Turbomachines, Ph.D. Thesis, Department of Aerospace Engineering, The Pennsylvania State University, University Park, Pennsylvania, USA, 1992.
[7] Th.H. Carolus, D.K. McLaughlin, R. Basile, Experimental investigation of the unsteady discharge flow field and the noise of a centrifugal fan impeller, The Seventh International Congress on Sound and Vibration Garmisch-Partenkirchen, Germany, 2000.
[8] D. Japikse, Turbomachinery diffuser design technology, Concepts ETI inc., Norwich, Vermont, 1984.
[9] M. Inoue, N.A. Cumpsty, Experimental study of centrifugal impeller discharge flow in vaneless and vaned diffusers, ASME Journal of Engineering for Gas Turbine and Power 106 (1984) 455–467.
[10] P.H. Bent, Experiments on the Aerodynamic Generation of Noise in Centrifugal Turbomachinery, Ph.D. Thesis, Department of Aerospace Engineering, The Pennsylvania State University, University Park, PA, USA, 1993.
[11] L.G. Mongeau, D.E. Thompson, D.K. McLaughlin, Sound generation by rotating stall in centrifugal turbomachines, Journal of Sound and Vibration 163 (1993) 1–30.
[12] L.G. Tetu, Experiments and Analysis of the Trailing Edge Aeroacoustics of Centrifugal Turbomachinery, Ph.D. Thesis, Department of Aerospace Engineering, The Pennsylvania State University, University Park, PA, USA, 1996.
[13] F.C. Gilman, Testing pumps as fan and fans as pumps, ASME Journal of Engineering for Power 90 (4) (1968) 140–143.
[14] J.-S. Choi, Experiments on the Unsteady Flowfield Associated with Noise Generation in Centrifugal Turbomachinery, Ph.D. Thesis, Department of Aerospace Engineering, The Pennsylvania State University, University Park, PA, USA, 1991.
[15] L.G. Mongeau, D.E. Thompson, D.K. McLaughlin, A method for characterizing aerodynamic sound sources in turbomachines, Journal of Sound and Vibration 181 (1995) 369–389.
[16] R.V. Westphal, R.D. Mehta, Crossed hot-wire data acquisition and reduction system, NASA TM-85871, 1984.
[17] C. Hah, B. Lakshminarayana, Effect of rotation on a rotating hot-wire sensor, Journal of Physics E 11(10) (1978).
[18] T.M.A. Maksoud, M.W. Johnson, Mean and turbulent flow measurements within the vaneless diffuser of a centrifugal compressor, Proceedings of the Institution of Mechanical Engineers, International Conference publications C263/87, 1987.
[19] R.C. Dean Jr., Y. Senoo, Rotating wakes in vaneless diffusers, ASME Journal of Basic Engineering 82 (3) (1960) 563–570.
[20] H.S. Fowler, The distribution and stability of flow in a rotating channel, ASME Journal of Engineering for Power, Series A 90 (1968) 229–236.
[21] D. Eckardt, Instantaneous measurements in the jet-wake discharge flow of a centrifugal compressor impeller, ASME Journal of Engineering for Power 97 (7) (1975) 337–346.
[22] M.W. Johnson, J. Moore, The influence of flow rate on the wake in a centrifugal impeller, ASME Journal of Engineering for Power 105 (1983) 33–39.
[23] L.G. Mongeau, Experimental Study of the Mechanism of Sound Generation by Rotating Stall in Centrifugal Turbomachines, Ph.D. Thesis, Department of Aerospace Engineering, The Pennsylvania State University, University Park, PA, USA, 1991.
[24] R.C. Dean, Jr., Boundary layers in centrifugal compressors, Fluid Mechanics, Acoustics, and Design of Turbomachinery, A symposium held at The Pennsylvania State University, University Park, USA, August 31–September 3, 1970.